CrossMark

Circular-to-linear polarization converter based on composite via-coupled patch frequency selective surfaces

Nan Shao[1] · Shen-Yun Wang[1] · Wen Geyi[1]

Abstract

In this paper, we present a design of circular-to-linear polarization converter operating in C-band based on a composite frequency selective surface which consists of two types of via-coupled patch modules. The building unit cell is built with four modules, and each one is a truncated patch pair printed on the double-layer substrate and vertically connected by a metal via-hole. A perforated common ground plane is sandwiched between the double layers to support transverse electric and magnetic mode coupling between the front and back patches. The front diagonally truncated patch array responds to the incident right-handed circularly polarized wave, and it is identically converted into general right- and left-handed elliptically or circularly polarized waves with same phase shifts, amplitudes and axial ratio, thus a resultant linear polarized wave is generated in forward transmission mode.

1 Introduction

Circularly polarized (CP) waves have many advantages, such as low susceptibility to the multipath, rain echo, and atmospheric effects of absorption and reflection. Thus, CP waves play important roles in modern satellite communication, navigation and some wireless local area networks [1]. For the mentioned wireless systems, CP waves can be directly generated using circularly polarized antennas, such as microstrip patch antennas [2], crossed-dipoles [3] and helix antennas [4]. An alternative approach of generating CP waves is to insert a linear-to-circular polarization converter on top of linearly polarized antenna or array, which can convert linearly polarized (LP) waves to CP ones effectively [5–8]. It has been proved that the latter way to generate CP waves shows a better flexibility, such as the handedness control using active reconfigurable CP wave converter [9, 10], and the antenna gain enhancement [5]. For this purpose, great efforts have been made to design CP wave converters using the so-called artificially engineered electromagnetic (EM) structures, such as the split-ring resonators [11–13], metasurfaces [14–16], substrate-integrated waveguide cavities

[17–19] and frequency selective surfaces [20–23]. When the linear-to-circular polarization converter is illuminated by a normally incident LP wave, two orthogonal linear wave components being of equal amplitudes and 90° phase difference are generated, resulting in a outgoing CP wave. Such working principle is on the basis of strong near electric and magnetic field coupling, and the conversion efficiency and bandwidth are usually limited.

Many investigations of the linear-to-circular polarization converters have been done for applications in transmitting CP antennas. However, to the best of our knowledge, little attention has been paid to the study of circular-to-linear polarization converter except the one presented in the literature [16], which works in optical regime. In fact, the circular-to-linear polarization converters play even more important roles in satellite communication systems. At the signal receiving end, when transmitting CP waves are converted into LP ones, the signal can be effectively received just using conventional LP antennas. It is known that when the CP waves are directly received by LP antennas, there exists 3.0 dB energy loss.

Here, we present a simple but novel approach to realize circular-to-linear polarization converters using a composite frequency selective surface (CFSS) structure. The design principle is first demonstrated to the best of our knowledge. Two kinds of via-coupled patch module are proposed to establish the building unit cell of the CFSS. Finally, for validating the proposed design, a prototype has been designed,

✉ Shen-Yun Wang
  wangsy2006@126.com

[1] Research Center of Applied Electromagnetics, Nanjing University of Information Science and Technology, Nanjing 210044, China

manufactured and measured and the working principle is discussed in detail.

2 Design schemes

To generate an outgoing LP wave from an incident plane CP wave (Here, we have assumed a RCP wave incidence), we try to identically convert the RCP wave into LCP and RCP ones, thus the outgoing RCP and LCP waves can be combined into a LP one when they are with same amplitudes and phase shifts. Based on this design principle, a CFSS structure is proposed with its building unit cell consisting of two kinds of polarization conversion modules, namely RCP-to-LCP and RCP-to-RCP conversion modules. In fact, much work has been done in the RCP-to-LCP polarization conversion using helix metamaterials [24–27] and asymmetrical chiral metamaterials [28]. Although helix metamaterials have advantages in wider operating bandwidth, they are usually 3-D structures, which implies difficult fabrication process and high cost.

To effectively receive the incident RCP wave, we take the conventional truncated patch antenna as the building component of the polarization conversion modules. Inspired by the thought that the frequency selectivity can be achieved using an array of antenna-filter-antenna (AFA) modules [29], which have been used to design the linear-to-circular polarization converters [22, 23], we replace the popular

aperture-filter directly by a via-hole, and a patch-via-patch (PVP) module is thus formed. That is to say, the PVP module is composed of a receiving patch antenna, a non-radiating via-hole structure passing through the perforated common ground plane, and a transmitting patch antenna. An analog of antenna-coaxial port-antenna module has been presented to realize a 3-D reflective linear polarization converter in our previous work [30], where the conversion principle can be understood as TE-to-TEM-to-TM mode conversion. Figure 1a, b schematically depict the circular-to-linear polarization converter, and the geometry of the patch component of the PVP module is shown in Fig. 1c. The building unit cell of the circular-to-linear polarization converter is built with four PVP modules and the front patch elements are denoted by A, B, C and D, and the back patches are denoted by A′, B′, C′ and D′, respectively, as shown in Fig. 1d, f. The common ground plane is periodically perforated to let the via-holes pass through as shown in Fig. 1e, and the connecting coaxial ports is formed to only support the transverse electric and magnetic (TEM) mode coupling, instead of the conventional high-order near electric and magnetic field coupling. Compared with the 3-D helix antenna, the truncated patch commonly operates in a narrow bandwidth. To overcome this limitation, a cross slot is etched within the truncated patch to somewhat enhance the operating bandwidth. For the A-to-A′ and B-to-B′ modules, the frequency response can be explained by an equivalent circuit model as illustrated in Fig. 2, where the patch antenna is treated an
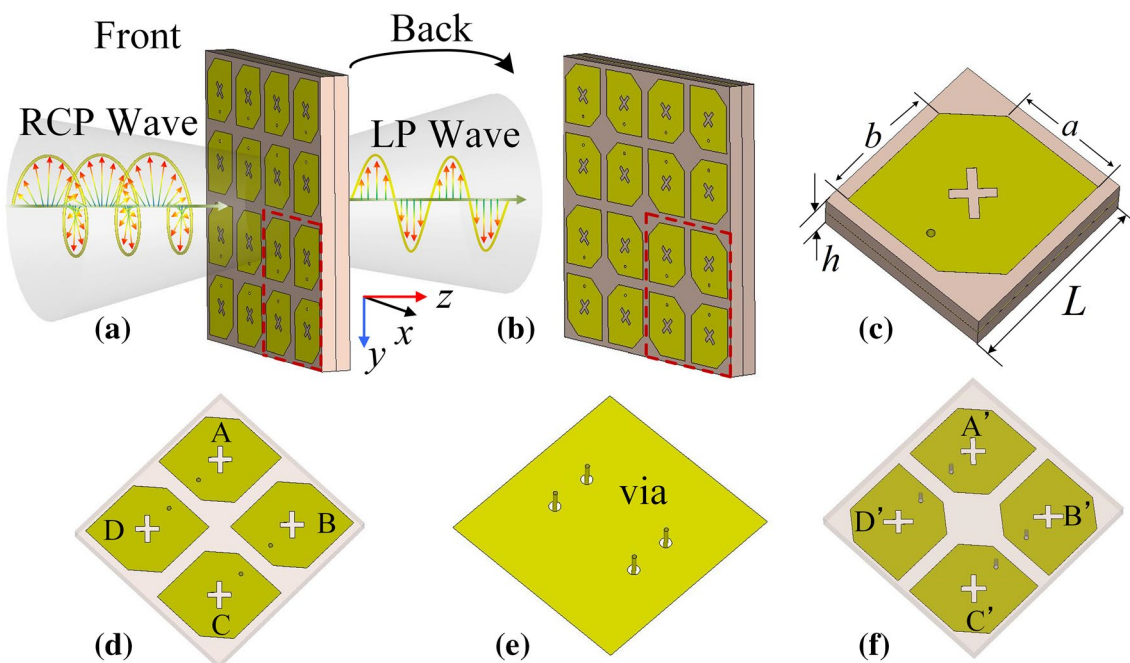
Fig. 1 The polarization converter **a** front view, **b** back view; **c** the via-coupled patch module; and the top view of **d** the top layer, **e** common ground plane and **f** back layer of the building element
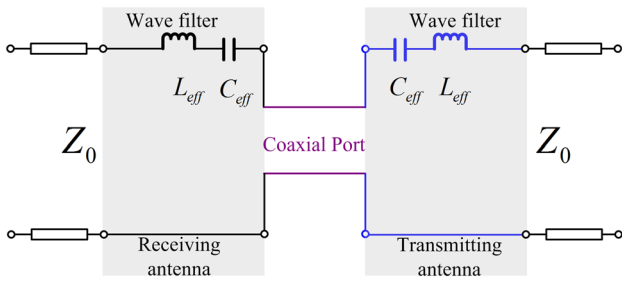
Fig. 2 Equivalent circuit model of the CP conversion module

LC circuit and the connecting coaxial-port supports TEM mode in the simulation frequency band. For the top and back patches being in same geometry, both kinds of the modules can be treated as one-order spatial filter and the frequency response is totally determined by the patch antenna itself.

The outgoing wave polarization and transmission coefficient are determined by the topological structure of the top and back patch elements, and the CP wave capture efficiency is dependent on the axial ratio (AR) of the patch element. If the top and back patch elements are both diagonally truncated, they function as a receiving RCP antenna and a transmitting LCP antenna, respectively, and such a module realizes the RCP-to-LCP polarization conversion, whereas if the top patch is diagonally truncated and the back patch is anti-diagonally truncated, such a module has function of RCP-to-RCP polarization conversion. As illustrated in Fig. 1a, for forward propagation, the incident RCP wave gives

$$\vec{E}_{\text{in\_RCP}} = \begin{pmatrix} I_x \\ I_y \end{pmatrix} e^{-jkz} = \begin{pmatrix} j \cdot E_0 \\ E_0 \end{pmatrix} e^{-jkz}. \tag{1}$$

The incident RCP wave is identically captured by the RCP-to-LCP and RCP-to-RCP modules within one unit cell, and the decomposed transmitted electric fields can be expressed as

$$\vec{E}_{t1} = \begin{pmatrix} T_{1x} \\ T_{1y} \end{pmatrix} e^{-jkz} = \begin{pmatrix} j \cdot k_x \cdot E_0 \\ k_y \cdot E_0 \end{pmatrix} e^{-jkz}$$
$$\vec{E}_{t2} = \begin{pmatrix} T_{2x} \\ T_{2y} \end{pmatrix} e^{-jkz} = \begin{pmatrix} -j \cdot k_x \cdot E_0 \\ k_y \cdot E_0 \end{pmatrix} e^{-jkz}, \tag{2}$$

where the coefficients k_x and k_y are mainly determined by the AR of the circularly polarized patch element of the modules in their response frequency band. When the patch antennas are working with their AR equal to one ($k_x = k_y$), the PVP modules have high CP wave capture and radiant efficiency. The total transmitted electric field can be obtained from Eq. (2),

$$\vec{E}_t = \vec{E}_{t1} + \vec{E}_{t2} = \begin{pmatrix} 0 \\ 2k_y \cdot E_0 \end{pmatrix} e^{-jkz}. \tag{3}$$

The supposed incident RCP wave given by Eq. (1) makes the converted LP wave polarized in y-axis as illustrated in Fig. 1a. Supposing that the RCP wave capture efficiency is unity, the parameters k_x and k_y approximately become 0.5, indicating a near unity LP wave conversion. When the AR of the patch antennas is unequal to one, the wave capture efficiency will decrease. However, it can be seen from Eq. (3) that the transmitted electric field still remains a highly purified LP wave component when the AR is unequal to one.

For backward propagation, the incident LP wave gives

$$\vec{E}_{\text{in\_LP}} = \begin{pmatrix} 0 \\ E_0 \end{pmatrix} e^{+jkz}. \tag{4}$$

and it can be decomposed into a RCP wave and a LCP one

$$\vec{E}_{\text{in\_RCP}} = \begin{pmatrix} I'_{1x} \\ I'_{1y} \end{pmatrix} e^{+jkz} = \begin{pmatrix} j0.5 \cdot E_0 \\ 0.5 \cdot E_0 \end{pmatrix} e^{+jkz}$$
$$\vec{E}_{\text{in\_LCP}} = \begin{pmatrix} I'_{2x} \\ I'_{2x} \end{pmatrix} e^{+jkz} = \begin{pmatrix} -j0.5 \cdot E_0 \\ 0.5 \cdot E_0 \end{pmatrix} e^{+jkz}. \tag{5}$$

The RCP wave component is converted into RCP one by the B′-to-B and D′-to-D modules, and the LCP wave component is converted into RCP one by the A′-to-A and C′-to-C modules in backward transmission modes

$$\vec{E}_{t1\_\text{RCP}} = \begin{pmatrix} T'_{1x} \\ T'_{1y} \end{pmatrix} e^{+jkz} = \begin{pmatrix} jk_x \cdot E_0 \\ k_y \cdot E_0 \end{pmatrix} e^{+jkz}$$
$$\vec{E}_{t2\_\text{RCP}} = \begin{pmatrix} T'_{2x} \\ T'_{2y} \end{pmatrix} e^{+jkz} = \begin{pmatrix} -jk_x \cdot E_0 \\ k_y \cdot E_0 \end{pmatrix} e^{+jkz}, \tag{6}$$

and the total transmitted electric field is thus given by

$$\vec{E}_{t\_\text{RCP}} = \vec{E}_{t1\_\text{RCP}} + \vec{E}_{t2\_\text{RCP}} = \begin{pmatrix} j2k_x \cdot E_0 \\ 2k_y \cdot E_0 \end{pmatrix} e^{+jkz}. \tag{7}$$

The transmission Jones matrix can be applied to relate the incident field to the transmitted field for both kinds of proposed modules. For the RCP-to-RCP module in forward transmission, we may write

$$\begin{pmatrix} T_{1x} \\ T_{1y} \end{pmatrix} = \begin{pmatrix} t_{1xx} & t_{1xy} \\ t_{1yx} & t_{1yy} \end{pmatrix} \begin{pmatrix} I_{1x} \\ I_{1y} \end{pmatrix}. \tag{8}$$

The reciprocal theorem is usually applied to derive the transmission matrix for the EM wave propagating along backward direction for polarization conversion array composed of one kind of module. Taking the RCP-to-RCP module working in backward transmission mode as an example, we have

$$\begin{pmatrix} T'_{1x} \\ I'_{1y} \end{pmatrix} = \begin{pmatrix} t_{1xx} & -t_{1xy} \\ -t_{1yx} & t_{1yy} \end{pmatrix} \begin{pmatrix} I'_{1x} \\ I'_{1y} \end{pmatrix}. \tag{9}$$

This indicates that the transmission energy is reciprocal for the building unit cell of the CFSS. However, seen from Eq. (7), the polarization states of the transmission wave are nonreciprocal except at the resonant frequency where the AR of the patches is equal to one ($k_x = k_y$), and a standard RCP wave can be generated when a LP wave is incident along the backward direction. When the patch elements are working with their AR unequal to one ($k_x \neq k_y$), the backward incident LP wave is converted into elliptically polarized one. For this reason, in this work, we mainly take the advantage of forward propagation to realize a circular-to-linear polarization converter in a wide frequency and AR band based on the proposed CFSS structure.

3 Results and discussion

In this study, the circular-to-linear polarization converter is optimized to operate at frequency of 5.8 GHz, and the dimensions of the building PVP module are found to be: $L = 14.0$ mm, $a = 8.3$ mm, $b = 9.4$ mm, $h = 3.083$ mm and $t = 0.035$ mm, where h and t represent the thickness of double-layer substrate and metal film, respectively, as shown in Fig. 1c. The substrate is Rogers RO4003 with dielectric constant of 3.55 and loss tangent of 0.0027, which leads to low insertion loss. The optimization and simulation are carried out using commercial software, Ansoft high frequency structure simulator (HFSS), and the frequency domain solver is chosen with periodic boundary conditions in both transverse directions, and the Floquet ports are used in the wave propagating direction to extract scattering parameters.

Here, we define the general reflection and transmission coefficients as R_{i-j} and T_{i-j}, respectively, where the indices i and j correspond to the polarization states of the outgoing and incident waves, respectively, which could be RCP wave, LCP and LP wave. Figure 3a shows the magnitudes

of the reflection and transmission when RCP waves normally impinge onto the presented polarization conversion device. Seen from the figure, a linearly polarized transmission (T_{LP-RCP}) response with its central resonant frequency at 5.8 GHz (nearly −0.21 dB) is obtained. The −3dB bandwidth ranges from 5.35 to 6.3 GHz (16% bandwidth). The circularly co- and cross-polarized reflections, namely $R_{RCP-RCP}$ and $R_{LCP-RCP}$, are less than −25dB at the resonant frequency, implying zero reflections. As mentioned in the above, the RCP wave is highly captured at the resonant frequency for the AR of the patches is equal to one.

To better evaluate the performances of the proposed polarization converter, the Ohm insertion loss (OIL) and relative conversion efficiency (RCE) have been calculated, respectively, using the following formulas:

$$OIL = 1 - |R_{RCP-RCP}|^2 - |R_{LCP-RCP}|^2 - |T_{RCP-RCP}|^2 - |T_{LP-RCP}|^2, \tag{10}$$

$$RCE = \frac{|T_{LP-RCP}|^2}{|R_{RCP-RCP}|^2 + |R_{LCP-RCP}|^2 + |T_{RCP-RCP}|^2 + |T_{LCP-RCP}|^2}. \tag{11}$$

The calculated result of *OIL* is shown in Fig. 3b, and the value at resonant frequency is less than 4.0% (about 0.2 dB, which is comparable to the cavity structures [18, 19]), and it tardily increases within the simulated frequency band. Because there is virtually no RCP and LCP reflections, and the absolute LP transmittance is approximately up to 96% at the resonant frequency. Ignoring the OIL, the RCE curve is also plotted in Fig. 3b, where a near unity RCE at the resonant frequency can be observed.

To validate the design, a prototype containing 12×12 building elements or 24×24 PVP modules is fabricated by utilizing the conventional printed circuit board technique. The measurement was carried out in an anechoic chamber and two RCP standard-gain horns, one LP receiving horn
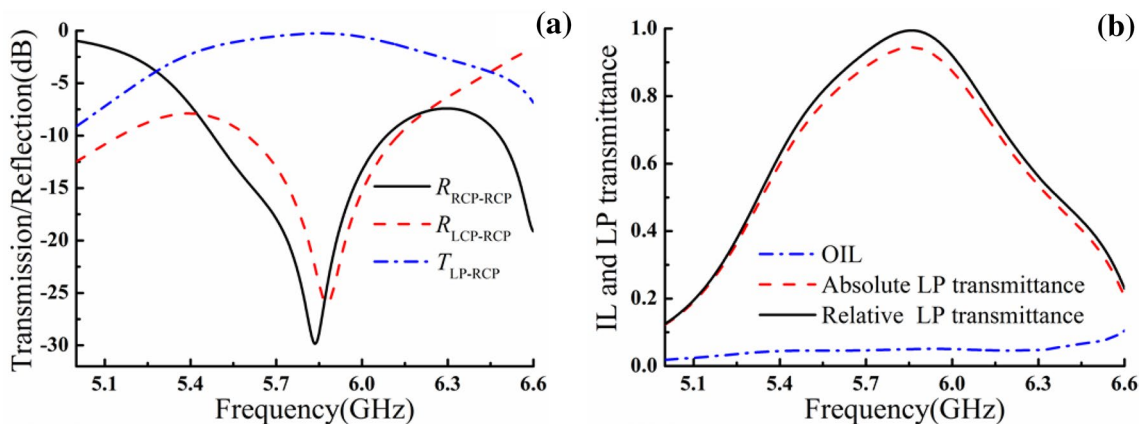
Fig. 3 **a** Amplitudes of the transmission and reflection of the polarization converter, **b** the Ohm insertion loss and LP polarization transmittance

and a vector network analyzer (VNA) were utilized, as shown in Fig. 4. For the RCP reflection measurement, two RCP horns are placed adjacently, while the sample locates at a certain far-field distance from the horns. During the LP transmission measurement, the RCP and LP horns are placed in the opposite sides of the sample. In both the cases, reference measurements have been recorded to normalize the imperfections during the measurements. The measured RCP reflection and LP transmission of the prototype are depicted in Fig. 5a, b, respectively, which show good agreement with the simulated responses. The deviations are acceptable and likely caused by the tolerances in fabrication and measurement.

To further understand the working principle of the presented polarization converter, we decompose the outgoing LP wave into RCP and LCP components (in fact, they are right- and left-handed elliptically polarized components with same amplitudes and AR). The phase shifts and amplitudes of the RCP and LCP waves are plotted in Fig. 6a, b, respectively. It can be found that both the phase and amplitude differences are close to zero in the simulated frequency band. This indicates that the incident RCP wave can be identically converted into RCP and LCP components and a standard outgoing LP wave is generated within the whole simulation frequency band. At the resonant frequency at 5.8 GHz, both the RCP and LCP amplitudes of the transmission wave are approximately -3.0 dB, representing an almost unity LP wave transmittance, as also demonstrated in Fig. 3a. At the non-resonant frequencies, the transmission amplitudes for LCP and RCP components are decreased. This is due to that the AR of the patch is unequal to one, resulting in lower capture efficiency of the incident RCP wave.

To gain an insight into the nature of the polarization conversion mechanism, the electric current distributions on the front and back patches at the resonant frequency are investigated. As shown in Fig. 7a, the current arrows are mainly

Fig. 4 Fabricated device sample and the experimental setup
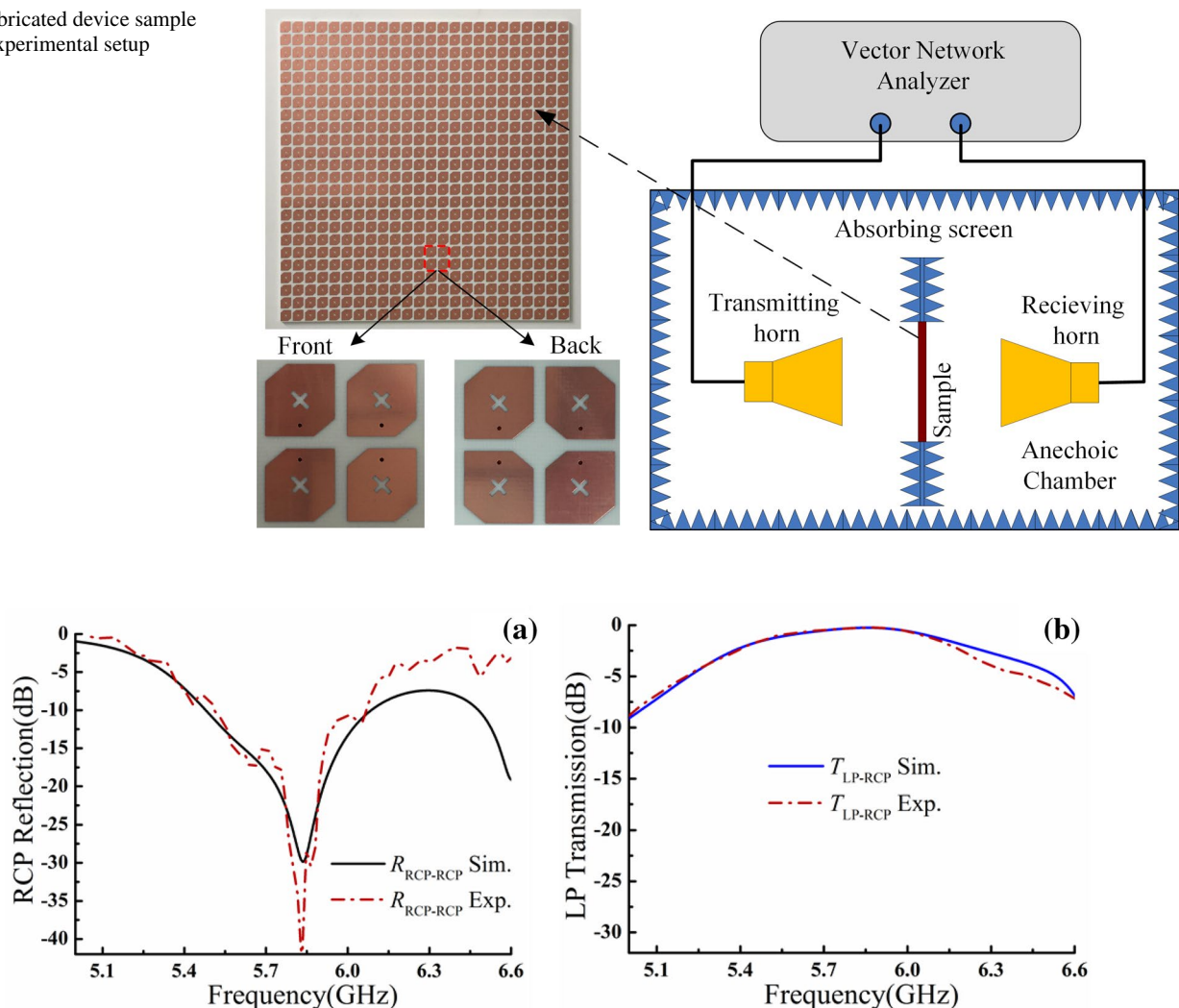
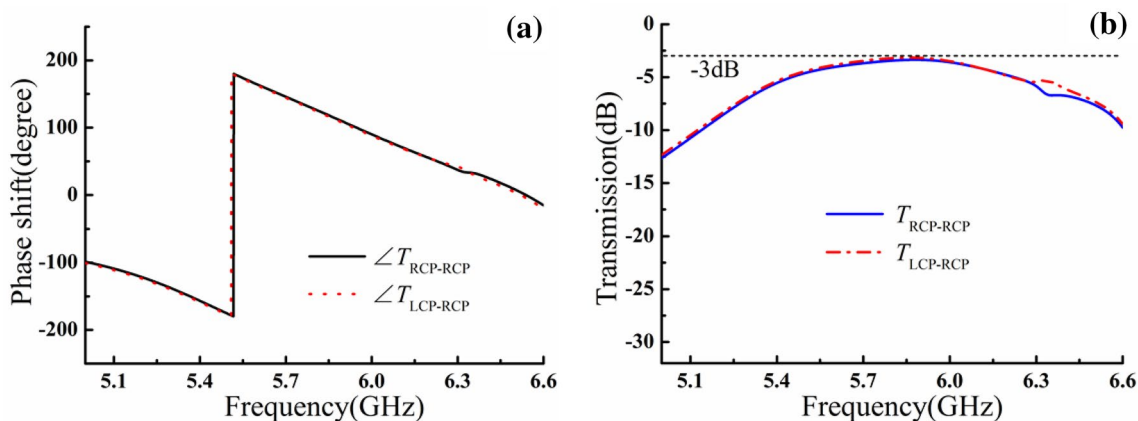**Fig. 5** **a** RCP reflection and **b** LP transmission obtained by experimental measurement and numerical simulation

Fig. 6 **a** Phase shift and **b** amplitudes of the LCP and RCP components of the outgoing LP wave
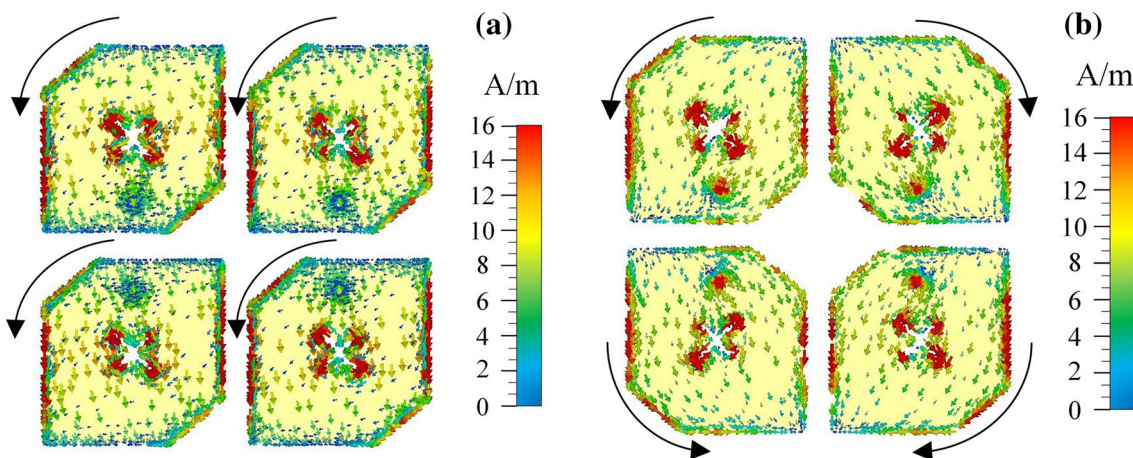

Fig. 7 Current distributions on **a** the front layer and **b** back layer at resonant frequency at 5.8 GHz

anticlockwise distributed on the edges of the front diagonally truncated patches, indicating the RCP wave response. However, on the back side of the building unit cell, the current arrow distributions remain the same as the top ones on the diagonally truncated patches (A′ and C′), but the current arrow distributions on the anti-diagonally truncated patches (B′ and D′) have an opposite direction. Therefore, the current distributions reveal that the incident RCP wave is identically converted into outgoing LCP and RCP components within one building unit cell and they are combined into a standard LP wave in forward transmission mode.

Ultimately, to demonstrate the reciprocity of the proposed device, a LP wave (linearly polarized in *y*-axis) is assumed to be incident from the backside. At first, we decomposed the transmitted wave into two orthogonal linear components, namely co-linearly polarized and cross-linearly polarized waves. The amplitudes and phase shifts

of the backward transmitted wave are shown in Fig. 8a, b, respectively. At resonant frequency 5.8 GHz, the amplitudes of the orthogonal linear components are both near −3.0 dB, and the phase shift of the co-linearly polarized component is 90° ahead of the cross-linearly polarized component, indicating that a transmitted RCP wave with both AR and conversion efficiency being of near unity is generated. At other frequencies, the amplitudes are unequal and phase difference is no longer 90°, resulting in an elliptically polarized wave, and the AR versus frequency is given in Fig. 8c. Thus, the polarization states of the transmission are nonreciprocal, but the amplitude of the transmission is reciprocal because the frequency response is only determined by the equivalent circuit of the identical patch elements. The forward and backward transmission amplitudes are simulated and plotted in Fig. 8d, and they are identical in the simulation band.
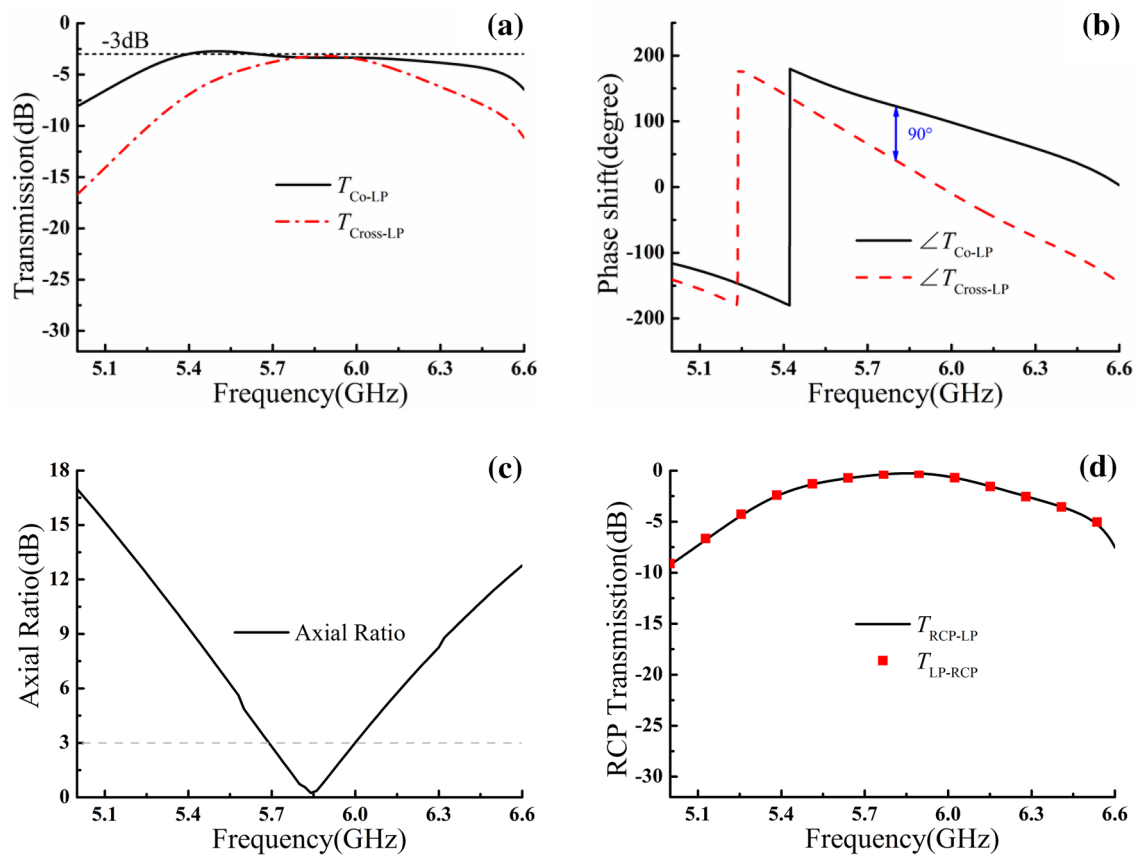
Fig. 8 **a** The amplitudes and **b** phase shifts of co- and cross-LP transmitted waves for LP-to-RCP conversion, **c** the AR of LP-to-RCP conversion versus frequency and **d** the amplitudes of the forward and backward transmissions

4 Conclusions

In summary, we have demonstrated a circular-to-linear polarization converter using a CFSS structure. The building unit cell of the CFSS consists of two RCP-to-LCP conversion modules and two RCP-to-RCP conversion modules. A prototype of the proposed polarization converter has been fabricated and tested, and all the measured results are in good agreement with the simulated ones, which validate the proposed design principle.

References

1. A. Kajiwara, IEEE Trans. Veh. Technol. **44**, 487 (1995)
2. S. Gao, Q. Luo, F. Zhu, Circularly polarized antennas. (Hoboken, Wiley, 2013)
3. Y.F. Lin, Y.K. Wang, H.M. Chen, Z.Z. Yang, IEEE Trans. Antennas Propag. **60**, 1221 (2012)
4. J. Dyson, IRE Trans. Antennas Propag. **7**, 181 (1959)
5. X.L. Ma, C. Huang, M.B. Pu, C.G. Hu, Q. Feng, X.G. Luo, Microwave Opt. Technol. Lett. **54**, 1770 (2012)
6. X.L. Ma, C. Huang, W.B. Pan, B. Zhao, J.H. Cui, X.G. Luo, IEEE Trans. Antennas Propag. **62**, 2307 (2014)
7. C. Zhang, Y.F. Wang, F.G. Zhu, G. Wei, J.Z. Li, C.Y. Wu, S. Gao, H.T. Liu, IEEE Trans. Antennas Propag. **65**, 385 (2017)
8. J.Y. Yin, X. Wan, J. Ren, T.J. Cui, Sci. Rep. **7**, 41505 (2017)
9. W.T. Li, S. Gao, Y.M. Cai, Q. Luo, M. Sobhy, G. Wei, J.D. Xu, J.Z. Li, C.Y. Wu, Z.Q. Cheng, IEEE Trans. Antennas Propag. **65**, 4470 (2017)
10. X.L. Ma, W.B. Pan, C. Huang, M.B. Pu, Y.Q. Wang, B. Zhao, J.H. Cui, C.T. Wang, X.G. Luo, Adv. Opt. Mater. **2**, 945 (2014)
11. J.Y. Chin, M.Z. Lu, T.J. Cui, Appl. Phys. Lett. **93**, 251903 (2008)
12. M. Euler, V. Fusco, R. Cahill, R. Dickie, IET Microw. Antennas Propag. **4**, 1764 (2010)
13. S. Yan, G.A.E. Vandenbosch, Appl. Phys. Lett. **102**, 103503 (2013)
14. H.L. Zhu, S.W. Cheung, K.L. Chung, T.I. Yuk, IEEE Trans. Antennas Propag. **61**, 4615 (2013)
15. J.D. Baena, J.P.D. Risco, A.P. Slobozhanyuk, S.B. Glybovski, P.A. Belov, Phys. Rev. B **92**, 245413 (2015)

16. Z.C. Li, W.W. Liu, H. Cheng, S.Q. Chen, J.G. Tian, Sci. Rep. **5**, 18106 (2015)
17. M.S.M. Mollaei, IEEE Antennas Wireless Propag. Lett. **16**, 1923 (2017)
18. J. Wang, W. Wu, Opt. Express **25**, 3805 (2017)
19. Z. Yu, S.Z. Xiang, F.Y. Jun, Chin. Phys. B **23**, 034101 (2014)
20. B.L. Li, Y.J. Li, Z. Wu, F.F. Huo, Y.L. Zhang, C.S. Zhao, Proc. IEEE 103, 1057 (2015)
21. P. Fei, Z.X. Shen, X. Wen, F. Nian, IEEE Trans. Antennas Propag. **63**, 4609 (2015)
22. B.Q. Lin, J.L. Wu, X.Y. Da, W. Li, J.J. Ma, Appl. Phys. A **123**, 43 (2017)
23. J.L. Wu, B.Q. Lin, X.Y. Da, K. Wu, Chin. Phys. B **26**, 094201 (2017)
24. J.K. Gansel, M. Thiel, M.S. Rill, M. Decker, K. Bade, V. Saile, G.V. Freymann, S. Linden, M. Wegener, Science **325**, 1513 (2009)
25. J.K. Ganse, M. Latzel, A. FrÓ§lich, J. Kaschke, M. Thiel, M. Wegener, Appl. Phys. Lett. **100**, 101109 (2012)
26. R. Ji, S.W. Wang, X.X. Liu, H.J. Guo, W. Lu, ACS Photonics **3**, 2368 (2016)
27. J. Wang, Z.X. Shen, W. Wu, Appl. Phys. Lett. **111**, 113503 (2017)
28. Z.Y. L.Wu, Y.Z. Yang, R.Z. Cheng, M. Gong, Y. Zhao, J. Zheng, Duan, X.H. Yuan, Appl. Phys. A **116**, 643 (2014)
29. A.A. Tamijani, K. Sarabandi, G.M. Rebeiz, IEEE Trans. Microwave Theory Tech. **52**, 1781 (2004)
30. P. Xu, S.Y. Wang, W. Geyi, J. Appl. Phys. **121**, 144502 (2017)